Concentration of Starlight from Large Apertures into a Single Spatial Mode for Long-Baseline Interferometry

Jeffrey A. Meisner

3113 40th Ave. S., Minneapolis, Mn. 55406; email: meis@minn.net; tel: 651-917-7528

Abstract. In order to perform accurate determination of fringe visibilities, the optical power entering a stellar interferometer should be present in a single spatial mode. However due to atmospheric phase variations, apertures much larger than the Fried parameter will not yield an increase in collected power using passive mode filtering (such as pinholes or optical fibers). The potential performance of a natural guide star adaptive optics system designed for the purpose of concentrating light from a large aperture into a single mode has been investigated using a hypothetical optical circuit which actively combines the power from subapertures in a binary tree structure. Theoretical performance limits based on the statistics of atmospheric turbulence and detector shot noise are presented, and compared with the results of simulations of such a system. It is concluded that an adaptive optics system with the predicted performance could very substantially increase the magnitude limit of a long-baseline stellar interferometer operating in the fringe-tracking mode.

1. Introduction

A long-baseline stellar interferometer can accurately determine underlying fringe visibilities only if interference over the entire pupil plane occurs in a single phase, or if the rms phase error over that area can be accurately determined. One simple and effective means of insuring this condition is by limiting the collecting aperture relative to the Fried parameter r_0. Although reducing the total collected optical power, small apertures ensure that the interfering beams have almost all of their power in a single spatial mode; interference can only occur between waves launched into the same mode. Interference occurring in other spatial modes will occur in random relative phases and not substantially contribute to the signal, yet the detected photons will still contribute shot noise. Not only will the signal-to- noise ratio not be augmented by the additional light collected by a large aperture, but calibration of visibility measurements will suffer as varying atmospheric conditions alter the amount of optical power in the intended spatial mode. Moreover, in the case of dim or weakly correlated sources, lack of a sufficient signal-to-noise ratio will prevent fringe-tracking and coherent integration of fringe visibility, greatly reducing the performance of the instrument when observing such objects.

Aside from limiting the primary apertures, spatial filtering can be obtained passively using pinholes (D. St-Jacques, 1998) or single-mode fibers (S. Shaklan, 1992). In either case, however, the amount of light accepted into a single mode is limited by the area over which the incoming wavefront is spatially coherent; increasing the aperture size much beyond r_0 will not increase the available power. Only active reduction in the magnitude of the wavefront phase variations through adaptive optics techniques can increase the power available in a single spatial mode (J.-M. Mariotti, 1994). The most basic adaptive optics system, tip-tilt correction, can appreciably augment the power present in the central mode, and is routinely employed in most interferometers. Higher order adaptive optics systems have the potential to further concentrate power into a single mode. Subsequent spatial filtering of the improved wavefront will select only the light present in the central mode, whose intensity has been increased according to the factor by which the Strehl ratio has been improved.

The hypothetical apparatus described in Section 2. concentrates light from a large aperture into a single mode, but in the opposite order. For each of 2^M subapertures, the collected light is first filtered into a single mode, and then the 2^M discrete optical signals are combined optimally in an optical circuit to produce a concentrated output. It can be surmised on the basis of general principles that the theoretical performance limits of the two configurations should be similar. However consideration of the discrete optical circuit reduces the complexity of the analysis from a system defined by three dimensions (beam cross-section and time) to one dimension (time only). We thus propose the optical circuit diagramed in Figure 1, not necessarily as a practical implementation, but rather as a means to investigate the fundamental capabilities of modal concentration using adaptive optics operating on a wavefront of collimated light distorted by transmission through atmospheric turbulence obeying Kolmogoroff statistics. Use of photon-counting detectors is assumed, with a specified quantum efficiency and a negligible rate of dark counts. The analysis has been limited to the more tractable narrowband case; wideband operation of such an apparatus is obviously desirable.

Sensitivity limits below which an adaptive optics system will have insufficient feedback to operate have been previously analyzed on the basis of very general principles (F. J. Dyson, 1975). Those order-of-magnitude results are consistent with the present conclusions which are based on the specific power spectrum of atmospheric delay noise, and supported with simulation results.

It's important to note that the configurations considered in this paper have been optimized according to the very specific goal of concentrating power into a single mode, rather than producing sharp images, the traditional goal of adaptive optics. An important point in this regard is the "power splitting" issue. An adaptive optical system designed for imaging the same wavelengths used for wavefront correction, must necessarily contain a beam splitter which reduces the portion of the light available for either the wavefront sensor or for the observation. In the present application, however, an optimal solution requires directing energy contained in the central mode to the output, and preferentially directing energy not present in the central mode to the wavefront detectors. The advantage of this approach is accentuated in the case of low-noise photon counting detectors where the presence of light present in the central mode entering the

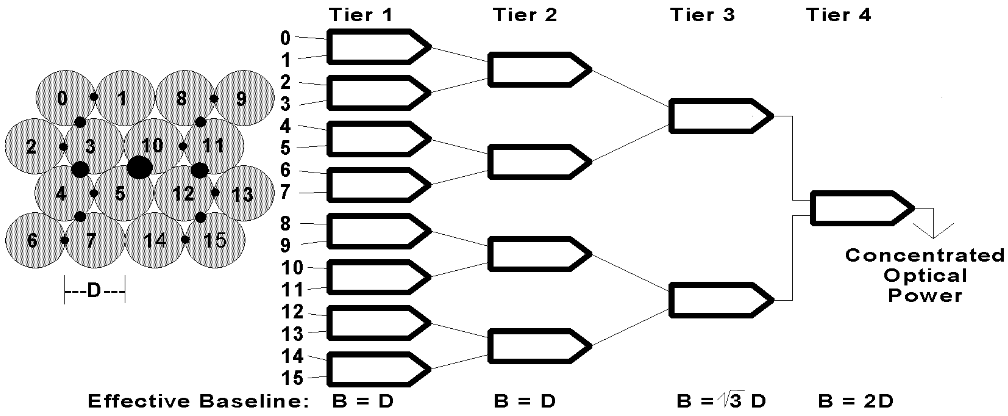

Figure 1. Optical power from an atmospherically perturbed wavefront is collected by a hexagonal array of subapertures (left). These are input into an optical circuit (right) in which power is concentrated as it propagates through a tree structure.

wavefront sensor not only robs energy from the intended output, but increases the shot noise level in the detectors. For the discrete optical circuit introduced below, this concern is addressed in the design of the photomixing network in (3) and the optimization of its design parameter θ.

The model for the discrete optical circuit is introduced in Section 2.. Design and analysis of the concentrator modules, the active components in the optical circuit, is briefly presented in Section 3.. In Section 4., the net performance of the concentrator tree using those results is predicted, and compared with the results of simulations. A number of approximations and limitations of the analysis are discussed.

2. Model

Consider the collection of light from a virtual point source by a square or hexagonal array of 2^M subapertures as depicted in the left side of Figure 1. Each subaperture collects a sample of the same wavefront subject to a random phase shift dependent on the column density of the atmosphere above that subaperture. The light from each subaperture is collected into an optical fiber or similar single-mode guided wave structure which enters an optical circuit for the purpose of concentrating the light received from the 2^M subapertures into a single mode. The active elements of that optical circuit, we shall call "concentrator modules."

Each concentrator module accepts two optical inputs derived from the same stellar source, but subject to a random relative phase shift ϕ. Depending on the mean optical level of the two inputs designated I_0, and the statistics of the phase function $\phi(t)$, a concentrator module will produce a mean output power of CI_0 where C is the "concentrating power" for that stage; perfect concentration corresponds to $C = 2$. The product of the concentrating powers applicable to each tier of the concentrator tree yields the net optical gain for the system. The

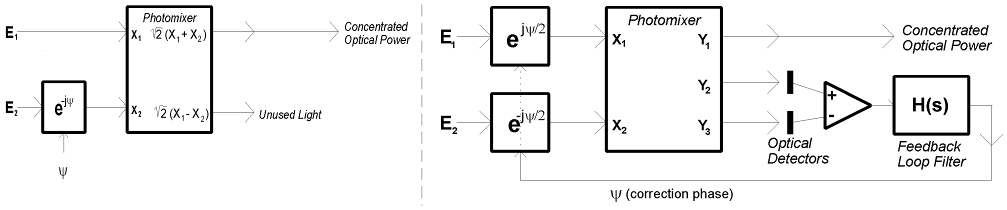

Figure 2. Left: Power from 2 optical signals can be combined following a phase correction. Right: Using a 3-output photomixer, a feedback signal can be generated to control the correction phase compensator.

ratio of that net concentrating power to the figure for perfect concentration 2^M, can loosely be identified as the "Strehl ratio" of the resulting adaptive optics system.

The statistics of ϕ for any stage are crucial in determining its performance. The concentrator modules of the first tier each receive inputs from adjacent subapertures laterally separated by a baseline of D. The concentrated light output from a first tier concentrator has a phase approximately the same as the phase of the wavefront at the midpoint of the two apertures; these positions are marked as small dots in Figure 1. Each of the second tier concentrators accept inputs whose phases therefore approximately correspond to the baseline (also of length D) between pairs of those points, producing an output whose phase is approximately the same as the phase of the wavefront at the midpoint of the those two points (shown as larger dots), and so on. At higher tiers, the effective baseline increases, increasing the magnitude of the low-frequency component of ϕ for those stages. According to atmospheric phase variations given by Kolmogoroff statistics, and the assumption of "frozen turbulence" driven by a wind of velocity V_0, the (2-sided) power spectrum of ϕ is approximately given by:

$$S_{\phi\phi}(f) = .0767 T_0^{-5/3} \frac{f^{-2/3}}{f^2 + f_b^2} \tag{1}$$

T_0 is a measure of the time scale of the atmospheric delay variations, and is defined as r_0/V_0. The low-frequency cutoff f_b, due to the baseline B, is approximately equal to $.204 V_0/B$ The increase in the magnitude of ϕ at the larger baselines sampled by the higher tiers, is mitigated by the larger input powers to those stages due to the concentration performed by previous stages of the concentrator tree.

3. The Concentrator Module

Consider two optical signals E_1 and E_2 , which differ only by the phase shift ϕ. Assume that the power of each signal is I_0. Then if an estimate of ϕ is available, the power of E_1 and E_2 can be combined using the network shown in Figure 2A. For the case of ψ, an estimator for ϕ, modeled as a gaussian random variable with a mean equal to ϕ and a variance of ϵ^2, the expected concentrating power would be:

$$C = \frac{E\{I_1\}}{I_0} = \frac{E\{I_0(1 + \cos(\psi - \phi))\}}{I_0} = 1 + e^{-\frac{\epsilon^2}{2}} \tag{2}$$

The optical power *not* concentrated into the upper output is available in the lower output. Unfortunately that power level is uncorrelated with the control error $\phi - \psi$, and thus cannot be used in a linear system to servo the delay compensator. The simplest photomixing network which efficiently concentrates optical power and also produces an acceptable output for generation of feedback to control the phase correction ψ has three optical outputs and is described by the following scattering matrix:

$$S = \begin{bmatrix} a_1 & a_1 \\ a_2 & -a_2 e^{j\theta} \\ a_2 & -a_2 e^{-j\theta} \end{bmatrix} \qquad a_1 = \sqrt{\frac{\cos\theta}{1 + \cos\theta}} \qquad a_2 = \sqrt{\frac{1}{2(1 + \cos\theta)}} \tag{3}$$

θ is a crucial design parameter which governs a trade-off between the maximum possible concentrated power available at Y_1, and the generation of a feedback signal through the optical power available at the Y_2 and Y_3 outputs of the photomixing network. The resulting concentrating power C thus obtained is plotted in Figure 3a for three different levels of uncorrected phase error. In the actual design of the concentrator module shown in Figure 3b, the optical outputs Y_2 and Y_3 are detected, subtracted, and run through a filter with the transfer function $H(s)$, to generate the phase correction ψ. Using an optimum filter transfer function, the predicted concentrating power C as a function of θ is plotted with solid lines in Figure 3b for normalized input power levels of 2, 4, 8, 16, 32 and 64. It is found that using a simple integrator of gain g for the filter, $H(s) = g/s$, achieves performance only slightly worse than that obtainable with the optimum filter; the predicted results using a simple integrator with g optimized are plotted with dashed lines. These plots are for a concentrator accepting signals with relative phase statistics corresponding to a baseline of r_0. Normalized optical power is defined as the number of photons per T_0, multiplied by the quantum efficiency of the feedback detectors. It should be pointed out that the theoretical performance depicted in Figure 3b is *not* borne out by simulations at the lower input power levels, as discussed below.

4. Net Performance and Simulation Results

For a given input power level to each subaperture, each tier of the concentrator tree receives an input power level determined by the accumulated power concentration of the prior stages. The filter transfer function $H(s)$ and θ for that tier are optimized on the basis of that expected input power. The accumulated power predicted at each tier of the concentrator tree is plotted logarithmically (in decibels) in Figure 4a for normalized input power levels of .32, 1.0, 3.2, and 10. At each stage the optimized value of θ in degrees is displayed. The calculated net concentrated output power for a 6, 8, or 10 tier concentrator tree as a function of incident flux on r_0-sized apertures in a hexagonal pattern is plotted in Figure 4b. A clear thresholding behavior is evident, below which concentration is impossible, corresponding to the lower flat curve in Figure 4a. Much

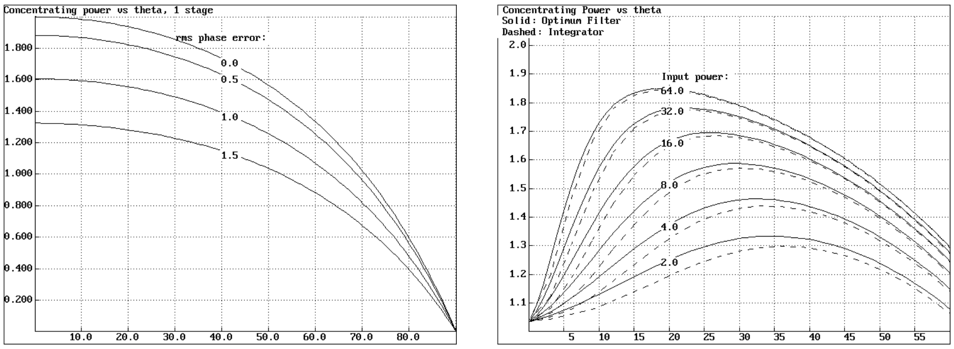

Figure 3. Left: Concentrating power as a function of the design parameter θ for phase correction errors of 0, .5, 1.0, and 1.5 radians rms. Right: Net system performance of a concentrator module as a function of θ for different input power levels. Dashed lines are predicted using a simple integrator for $H(s)$

above the threshold of 2 photons per r_0^2 per T_0, a rapid increase in the gain of the system is predicted.

Results of simulations using randomly generated photons are plotted as bold lines in Figure 4a and as x's in Figure 4b, showing performance inferior to the theoretical curves. According to the simulations, achieving the gains predicted by theory requires approximately 2.5 times the input light level specified by the formulae. The threshold for optical concentration occurs at around 5 photons per r_0^2 per T_0 (for detectors with unity quantum efficiency).

Among the approximations affecting the theoretical performance is the small signal approximation $sin(x) \approx x$ for the phase error. At low light levels the rms error of the phase correcting servo in Figure 2 exceeds unity. A important effect not accounted for in the theoretical analysis (but included in the simulations) is the generation and propagation of intensity variations induced by each concentrator module as the instantaneous correction phase error fluctuates.

A major shortcoming of both the theory and simulations is the narrowband assumption. Although the *correction* aspect of the concentrator modules using true delay compensators is inherently wideband, the interferometric detection as depicted in Figure 2b suffers complications when analyzed from the standpoint of white light, and the effect of 2π phase jumps on the concentration of wideband light has been neither simulated nor adequately analyzed. It is possible that multi-spectral detection of the feedback signals could be employed to reduce or eliminate 2π ambiguities using techniques previously developed for fringe tracking in long-baseline interferometry (Meisner, 1996).

On the positive side, the stipulation of each concentrator module operating independently of all others, while greatly simplifying the analysis, fails to take advantage of correlations between the phases of nearby subapertures that are not paired in the topology of Figure 1 (for instance, subapertures 1 and 8). While it is expected that utilizing the *a priori* correlation between the atmospheric delays affecting such subapertures would only contribute modestly to the narrowband

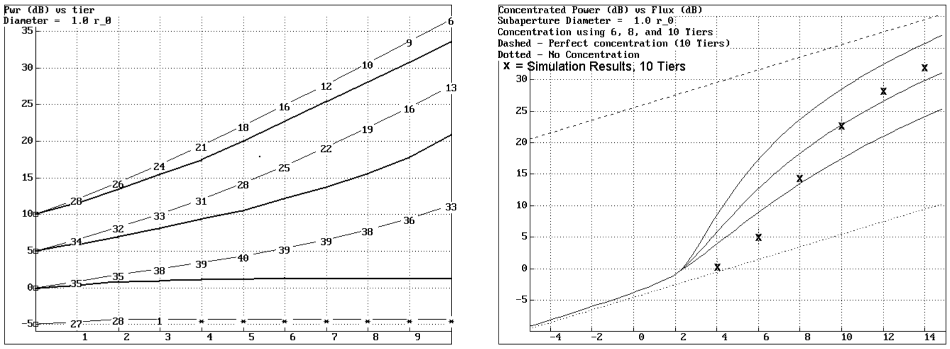

Figure 4. Left: Increase in power along a 10-tier concentration tree, at 4 different input power levels. Solid lines are simulation results. Right: Output power from a 6, 8, or 10-tier concentration tree as a function of input flux; 0 dB = 1 photon per r_0^2 per T_0 with unity quantum efficiency detectors. 'x' = simulation results (10-tier concentration tree). Subaperture diameter = r_0

performance of the system as analyzed, it could contribute very substantially to resolving 2π ambiguities in a wideband system, since the *a priori* probability of a full wavelength difference between the signals received at subapertures separated by r_0 is quite small.

5. Conclusion

Analysis of a hypothetical discrete-mode optical circuit has derived relationships between the power input into and extracted from an adaptive optics system optimized for the concentration of optical power into a single spatial mode. Simulations have shown performance at the levels predicted for input power levels about 2.5 times greater than specified by formulae. If the complications associated with wideband operation are not severe, these results would predict a threshold magnitude of about $m_v = 14$ for such a system assuming $r_0 = 10$cm, an effective wind velocity $V_0 = 5$m/sec, and detectors with a 30% quantum efficiency. Such an apparatus would substantially extend the magnitude limit of a long-baseline interferometer in the fringe-tracking mode even for unresolved sources.

Further details of the analysis and conclusions presented in this paper can be found on the internet at the following location:

http://www1.minn.net/~meis/concentration

References

S. Shaklan, M. Colavita, M. Shao 1992, High-Resolution by Interferometry II, ESO Proc. Vol. 39, 1271

D. St-Jacques, J. E. Baldwin, R. C. Boysen, C. A. Haniff, P. R. Lawson, J. Rogers, P. J. Warner, D. M. A. Wilson, J. S. Young 1998, Astronomical Interferometry, Proc. SPIE Vol. 3500, 762

J.-M. Mariotti 1994, in Adaptive Optics for Astronomy, ed. D. M. Alloin, J.-M. Mariotti, Kluwer Academic Publishers, 309

F. J. Dyson 1975, J. Opt. Soc. Am., 65, 551

J. Meisner 1996, Optical Engineering, 35, 1927